Edge state behavior of interacting bosons in a Su-Schrieffer-Heeger lattice

A. Ghosh [1,2] and A. M. Martin [1]
[1]School of Physics, University of Melbourne, Melbourne 3010, Australia
[2]Indian Institute of Technology Kharagpur, Kharagpur, West Bengal 721302, India

(Received 23 October 2024; accepted 22 January 2025; published 14 February 2025)

In the low-energy regime, the Su-Schrieffer-Heeger (SSH) model's key characteristics are encapsulated by a Dirac-type Hamiltonian in continuum space, i.e., localized states emerge at the boundaries. Building on this, we have developed an effective Hamiltonian to model ultracold interacting bosons on an SSH-like lattice through variational minimization under the mean-field approximation. To pinpoint the boundary states, we have developed an algorithm by generalizing the imaginary time propagator, where an initial state evolves under the squared Hamiltonian to converge to the targeted state. This algorithm has broader applicability, enabling the identification of specific eigenstates in various contexts. Furthermore, we draw a parallel to an experimentally physical setup involving a gas of ultracold bosons confined to an array of potential wells with alternating depths. By establishing the system's analogy with the SSH system, we apply our algorithm to investigate boundary states in the presence of interactions, demonstrating how these findings align with those of the continuous system.

DOI: 10.1103/PhysRevResearch.7.013169

I. INTRODUCTION

Topological physics represents a dynamic frontier within condensed matter physics [1–5]. In these systems, there is a topology associated with the bulk, depending on the symmetries present, giving rise to exotic edge/boundary properties, a phenomenon referred to as bulk-boundary correspondence [6–8]. The properties of edge states are critically significant and can manifest in diverse contexts, such as in the Su-Schrieffer-Heeger (SSH) model, the quantum Hall effect, the quantum spin Hall effect, and higher-dimensional topological insulators etc. [6–12]. The experimental realization of various topological phases has generated considerable excitement and holds great promise [13–17]. Numerous techniques have been employed to probe topological states, advancing our understanding and paving the way for innovative applications [18–20]. These systems are implemented through a variety of platforms, including optical lattices, where ultracold atoms are manipulated in controlled environments, photonic systems that guide light through engineered structures, and diverse solid-state materials that provide unique opportunities to explore and exploit topological phenomena [21–23]. Additionally, topological phases are being studied in classical systems outside the quantum regime, such as electrical networks and metamaterials [24,25]. The Su-Schrieffer-Heeger (SSH) model [6,7,26], a foundational framework for hosting topological phases, has been successfully implemented in experimental settings [17,21,22]. These studies naturally raise the intriguing question of how boundary states in the SSH system, primarily determined by a single-particle Hamiltonian, transform with the introduction of interactions. Several recent studies have investigated this phenomenon across various scenarios and settings [27–29]. For example, [27] examined the impact of interactions on topological edge states in spinful fermions, specifically examining the Su-Schrieffer-Heeger-Hubbard (SSHH) model. Similarly, [28] explored this scenario in the context of the Bose-Hubbard model, while [29] examined the persistence of topological characteristics amid competition from chiral symmetry-breaking potentials and on-site interaction terms in a tight-binding setup.

Leveraging recent breakthroughs in ultracold physics that have unlocked the ability to create condensates in nonground states using cesium atoms [30], in this paper, we shed light on the fate of the boundary states in a dilute gas of interacting bosons in ultracold settings on an SSH-like lattice. The emphasis is on boundary states, investigated using a constructed effective Hamiltonian, which we analyze using a developed algorithm.

The SSH lattice under low-energy regime is described by a continuum Dirac-type Hamiltonian [7,31], which captures the highly localized states at the boundary. Taking this into account, in Sec. II, we employ a mean-field approximation and perform variational minimization of the energy functional to obtain an effective Hamiltonian for the system, assuming contact interactions between particles corresponding to the *s*-wave scattering. This Hamiltonian, as a derivative of a Dirac-type Hamiltonian, can host a spectrum of eigenvalues, both positive and negative. As the conventional imaginary time algorithm probes for the lowest eigenvalue [32], in Sec. III A, we develop an algorithm to pinpoint a particular eigenstate in order to study the boundary state. In Sec. III B, we prepare the ground for the application of this algorithm to this particular problem. In Sec. IV A, we explore boundary states across a range of interaction strengths and boundary

Published by the American Physical Society under the terms of the Creative Commons Attribution 4.0 International license. Further distribution of this work must maintain attribution to the author(s) and the published article's title, journal citation, and DOI.

sharpness levels, comparing these findings to the cases where no interactions are present. To cultivate an intuitive and physically meaningful comprehension of the results, Sec. IV B investigates a related scenario involving bosons in a periodic well-like lattice with staggered amplitudes. After demonstrating its analogy to the SSH system, we proceed to apply the developed algorithm to investigate the boundary eigenstates in the presence of interactions. These eigenstates are analyzed using the Gross-Pitaevskii equation, allowing us to draw insightful parallels between the two systems. Finally, in Sec. V, we provide a comprehensive summary and conclusions of our findings.

II. EXPLORING CONTINUUM MECHANICS IN A SSH SYSTEM WITH INTERACTIONS

A discrete tight-binding system such as the SSH system can be treated as a continuous system under an appropriate regime., i.e., under low-energy approximation [6,31]. This continuum model also explains the presence and localization of edge states at the boundary between two distinct topological regimes. The central idea here is to incorporate interactions and develop an effective model for describing the bosonic interacting bosonic SSH system, enabling the study of edge states. To begin with, we provide a brief overview of the continuum treatment of the SSH system. As a starting point, the SSH Hamiltonian ($\hat{H}$) in discrete space is given by

$$\hat{H} = v\sum_{m=1}^{m=N} |m,A\rangle\langle m,B| + w\sum_{m=1}^{m=N-1} |m,A\rangle\langle m+1,B| + \text{H.c.}, \tag{1}$$

where m denotes the index of the unit cell, which is composed of sublattices A and B, linked by staggered hopping amplitudes. The parameter v corresponds to the intracellular hopping amplitudes, while w represents the intercellular hopping amplitudes. Translational invariance allows us to write the Hamiltonian in momentum space using $|K\rangle = |k,\alpha\rangle$ for $\alpha \in \{A,B\}$,

$$\hat{H}(k) = [v + w\cos k]\hat{\sigma}_x + w\sin k\hat{\sigma}_y. \tag{2}$$

Considering points in the momentum space close to the point of closure of the band ($q = k - k_0$), we have

$$\hat{H}(q+k_0) = [v + w\cos(q+k_0)]\hat{\sigma}_x + w\sin(q+k_0)\hat{\sigma}_y. \tag{3}$$

When $q \approx 0$ and $k_0 = \pi$,

$$\hat{H}(q) = [v - w]\hat{\sigma}_x - wq\hat{\sigma}_y. \tag{4}$$

In continuum treatment of a discrete system, q is replaced by the corresponding operator $-i\hbar\partial/\partial x$, treating the space as continuous so that $|\psi_{\text{Discrete}}\rangle = \sum_m \phi(x=m)|m\rangle$, if $\phi(x)$ is the solution in continuum space. This is known as the envelope-function approximation [6]. For this to hold, the wavefunction in momentum space must be confined well within the boundaries of the first Brillouin zone. Here, we get a Dirac-type equation (4) with a mass term $M = v - w$. For the case when $v = w$, the mass term vanishes, and we obtain a linear dispersion relation. The boundary between systems of different topological constants hosts an edge state, and this fact is also reflected through Eq. (4). Specifically, when we have a change in sign in M (v goes from less than w to greater than w), theoretical calculations show there is an edge state on the boundary with exponential decay [6,31]. Since we intend to examine the edge state under interactions, we will address this through numerical methods, as discussed in Sec. III.

Under the assumptions of this model, if there are N_p interacting bosons, the total Hamiltonian is given by

$$\hat{H} = \sum_{i=1}^{i=N_p} M_i\sigma_x - wq_i\sigma_y + \frac{1}{2}\sum_i\sum_j V(x_i - x_j)\times I. \tag{5}$$

In order to obtain the effective governing equation for the system, we treat the Hamiltonian in a mean-field manner by considering the ansatz wavefunction,

$$\Psi = \psi_1 \otimes \psi_2 \otimes \ldots \otimes \psi_{N_p-1} \otimes \psi_{N_p}. \tag{6}$$

Here, ψ_n represents the wavefunction of the nth particle and is expressed as a 2×1 matrix as a function of x_n, where the two components correspond to the two sublattices. Minimizing the functional $\langle\Psi|\hat{H}|\Psi\rangle$ respecting the constraint $\langle\Psi|\Psi\rangle = 1$, which in coordinate space is

$$\int \psi_1^\dagger \otimes \ldots \otimes \psi_{N_p}^\dagger \Bigg[\sum_{i=1}^{i=N_p} M_i\sigma_x - wq_i\sigma_y + \frac{1}{2}\sum_i\sum_j V(r_i - r_j)\times I\Bigg]\psi_1 \otimes \ldots \otimes \psi_{N_p} dx_1..dx_{N_p}. \tag{7}$$

For ultracold bosons, all particles acquire the state ψ, so the first term in Eq. (7) simplifies to $N_p\int \psi^\dagger M\hat{\sigma}_x\psi dx$. The second term, after applying integration by parts, reduces to $-N_p w\int i\hbar\frac{d\psi^\dagger}{dx}\hat{\sigma}_y\psi$. For dilute gases at low temperatures, the interaction can be described by $V(x) = \alpha\delta(x)$. Thus, the third term in the integral is given by $\frac{N_p(N_p-1)}{2}\int \psi_i^\dagger\psi_j^\dagger\alpha\delta(x_i - x_j)\psi_i\psi_j dx_i dx_j$. Thus, minimizing of the functional in Eq. (7) leads to

$$\delta\int\Big[N_p\psi^\dagger M\hat{\sigma}_x\psi dx - N_p wi\hbar\frac{d\psi^\dagger}{dx}\hat{\sigma}_y\psi + \frac{N_p^2}{2}\alpha\psi^\dagger\psi^\dagger I\psi\psi - EN_p\psi^\dagger\psi\Big]dx = 0. \tag{8}$$

Applying Euler-Lagrange equation, $\partial J/\partial\psi^\dagger - \partial/\partial x(\partial J/\partial\psi_x^\dagger) = 0$, we obtain the mean-field equation for the interacting bosons on an SSH lattice,

$$[M\hat{\sigma}_x - wq\hat{\sigma}_y + \alpha'|\psi|^2 I]\psi = E\psi. \tag{9}$$

In the above discussion, J is the functional in Eq. (8), and α' is $N_p\alpha/2$.

Equation (9)—a massive Dirac-type equation enhanced by a nonlinear term representing interacting bosons on an SSH lattice—will enable us to explore the edge states, as will be discussed in Sec. IV. Since the Dirac equation has infinitely many negative eigenvalues, it is difficult to obtain the eigenstates corresponding to the near-zero-energy eigenstates by using the imaginary time propagation algorithm alone. To address this problem, we develop an algorithm to compute a specific eigenvector, which is particularly useful when it is not in the ground state. Furthermore, we apply the algorithm

to solve a physically intuitive continuum system with similar physical properties, as is discussed in Sec. IV B. The next section (Sec. III) presents the algorithm.

III. INTRODUCTION TO THE ALGORITHM OF IMAGINARY TIME PROPAGATOR UNDER SQUARED HAMILTONIAN

A. The algorithm

The focus here is on the localized states at the boundary and the impact of interaction on them; however, Eq. (9) hosts states with both negative and positive eigenvalues. The widely used imaginary-time propagator algorithm is designed to provide the eigenvector corresponding to the lowest eigenvalue [32]. For the sake of completeness, the basic principle of operation may be stated as follows: For a system, $\hat{H}\psi = E\psi$, where E satisfies $E_1 < E_2 < E_3 \ldots$, a trial wavefunction evolves as $\psi(t) = \sum_n c_n e^{-itE_n}\psi_n$, where c_n is the overlap between the trial state and the nth true state of the system. If we consider the imaginary time, i.e., $\tau = it$, then $\psi(t) = \sum_n c_n e^{-\tau E_n}\psi_n$. As τ increases, the contribution from higher-energy terms decays faster than the lowest-energy term. After a sufficient number of steps, with normalization at each step, the lowest-energy state becomes exponentially enhanced.

The algorithm described below addresses this shortcoming. The basic idea is to update the wavefunctions using $\hat{H}^2$ corresponding to the square of energy. Specifically, for $\hat{H}\psi = E_0\psi$, the trial wavefunction ψ_0 is updated at each step using $(\hat{H} - E_0)^2$ to reach eigenvector ψ corresponding to the lowest eigenvalue close to zero, for close enough trial E_0 for the desired eigenvector. Consider the increment ψ with respect to the imaginary time parameter in the direction of the negative gradient of the square of energy in wavefunction space,

$$\frac{\partial|\psi\rangle}{\partial\tau} = -\frac{1}{2}\frac{\partial E^2}{\partial|\psi\rangle}. \tag{10}$$

Noting $E = \langle\psi|\hat{H}'|\psi\rangle = \langle\psi|\hat{H} - E_0|\psi\rangle$, we obtain, $\frac{\partial|\psi\rangle}{\partial\tau} = \hat{H}'^2|\psi\rangle$, leading to the time evolution as

$$|\psi(\tau + \delta\tau)\rangle \approx \left[\frac{I - \delta\tau \times \hat{H}'^2}{I + \delta\tau \times \hat{H}'^2}\right]|\psi(\tau)\rangle, \tag{11}$$

and the convergence is achieved when $\partial|\psi\rangle/\partial\tau \approx 0$, i.e., $E(\tau + \delta\tau) \approx E(\tau)$. Figure 1 depicts the steps involved in the imaginary-time propagator under the squared Hamiltonian (ITPUSH) algorithm, which is used to analyze the boundary state of interacting ultracold bosons on an SSH lattice. The value of E_0 and the trial wavefunction, obtained by solving the noninteracting case using the finite-difference method, are fed into Eq. (11) for iteration until convergence is reached, which is subjected to verification using the stability of the probability density under real-time evolution of the wavefunction ($\psi(t) = \sum_n c_n e^{-itE_n}\psi_n$). The interaction strength is gradually increased, with the wavefunction from the previous interaction strength as the trial wavefunction. The following subsection demonstrates the application of this algorithm to study the boundary states of interacting bosons in an SSH lattice.

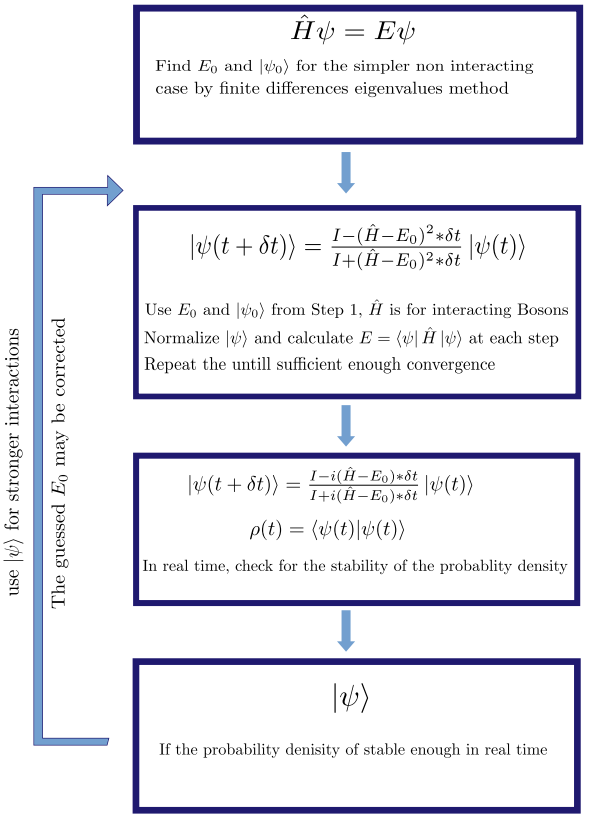

FIG. 1. Flow chart illustrating the implementation of the algorithm to identify the boundary localized state of interacting bosons in an SSH lattice, whose energy lies embedded within the system's energy spectrum.

The significance of the algorithm lies in its ability, in principle, to reach any desired target state, provided the trial wavefunction ψ_0 and the energy E_0 are sufficiently close. The selection of E_0 must ensure that its difference from the actual energy is smaller than its difference from any nearby energy levels.

B. The implementation

Our strategy involves setting up the matrix equation $H\psi = E\psi$ for the system, and then moving on to determine the H^2 term for use in the ITPUSH algorithm. To begin with, the matrix form of Eq. (9) is

$$\begin{bmatrix} \alpha'(|\psi_a|^2 + |\psi_b|^2) & M + w\frac{\partial}{\partial x} \\ M - w\frac{\partial}{\partial x} & \alpha'(|\psi_a|^2 + |\psi_b|^2) \end{bmatrix}\begin{bmatrix}\psi_a \\ \psi_b\end{bmatrix} = E\begin{bmatrix}\psi_a \\ \psi_b\end{bmatrix}. \tag{12}$$

The expression for H^2 is then given by

$$\begin{bmatrix} \gamma^2 + M^2 + w\frac{\partial M}{\partial x} - w^2\frac{\partial^2}{\partial x^2} & 2\gamma M + 2\gamma w\frac{\partial}{\partial x} + w\frac{\partial\gamma}{\partial x} \\ 2\gamma M - 2\gamma w\frac{\partial}{\partial x} - w\frac{\partial\gamma}{\partial x} & \gamma^2 + M^2 - w\frac{\partial M}{\partial x} - w^2\frac{\partial^2}{\partial x^2} \end{bmatrix}\begin{bmatrix}\psi_a \\ \psi_b\end{bmatrix} = E^2\begin{bmatrix}\psi_a \\ \psi_b\end{bmatrix}, \tag{13}$$

where $\gamma = \alpha'(|\psi_a|^2 + |\psi_b|^2)$. This leads us to coupled differential equations in ψ_a and ψ_b. To solve for $\psi = [\psi_a \quad \psi_b]^T$, under the ITPUSH algorithm we write ψ as

$$\psi_a \otimes [1 \quad 0]^T + \psi_b \otimes [0 \quad 1]^T, \tag{14}$$

and $\hat{H}$ as

$$\hat{H} = \hat{H}_{11} \otimes \begin{bmatrix} 1 & 0 \\ 0 & 0 \end{bmatrix} + \hat{H}_{12} \otimes \begin{bmatrix} 0 & 1 \\ 0 & 0 \end{bmatrix} + \hat{H}_{21} \otimes \begin{bmatrix} 0 & 0 \\ 1 & 0 \end{bmatrix} + \hat{H}_{22} \otimes \begin{bmatrix} 0 & 0 \\ 0 & 1 \end{bmatrix}. \tag{15}$$

In the above steps, the space is discretized into a grid of N_g points, making ψ and $\hat{H}$ correspond to a grid of $2N_g$ and $2N_g \times 2N_g$points, respectively. This enables us to calculate for ψ_a and ψ_b simultaneously using the algorithm. As discussed in the previous subsection, after sufficient convergence in E using Eq. (11), the obtained ψ is verified by evolving in real time for stability of the probability density under the Hamiltonian $\hat{H}$ [Eq. (12)]. We then proceed to a stronger interaction, using the result from the current interaction as the input for the algorithm, and this cycle is repeated.

IV. RESULTS AND DISCUSSION

A. Case of continuum SSH system

In this section, we apply the developed algorithm to a system with a boundary, specifically when there is a sign change in $M(x)$ $(= v - w)$ along the length of the system, see Fig. 2(b). We begin by investigating the case where no interaction is present, i.e., $\alpha' = 0$. The boundary of the domains can have different patterns, which we denote by the parameter β, such that $M(x)$ is given by $M(x) = -M_0 \tanh(\beta x)$. This parameter quantifies the steepness of the domain wall. Drawing from the discrete model [Eq. (1)] and analytical studies of continuum treatments of the SSH system [6,7,31], it is well established that the boundary states possess zero energy. Accordingly, we set $E_0 = 0$ in the ITPUSH algorithm to obtain the corresponding wavefunction. This choice aligns with the theoretical predictions and ensures that the algorithm accurately captures the characteristics of the boundary states. Figure 2(a) visualizes localized states at the domain boundary, underscoring a critical characteristic: the extent of localization is governed by the sharpness of the boundary. Specifically, sharper boundaries result in more localized states, while flattened boundaries result in greater delocalization. This relationship offers key insights into the behavior of boundary states. Importantly, across all cases examined, the ψ_b consistently remains zero. As detailed in Sec. III, the verification of the converged wavefunction is verified by its stability during real-time evolution under $\hat{H}$. This is exemplified in Fig. 2(c), where the probability density corresponding to ψ_a remains constant throughout the real-time evolution of the wavefunction, demonstrating its robustness and accuracy.

Next, we consider the scenario where interactions are present in the system, with the mean-field governing equation described by Eq. (9). The algorithm is again applied; in this instance, we initiate the process by utilizing the wavefunctions ψ_a and ψ_b derived from the noninteracting case as the initial state for our analysis. The impact of the interaction is illustrated by adjusting its strength across two distinct levels of boundary sharpness, see Fig. 3. This variation allows observation of how the interaction influences the system under different boundary conditions. Unlike the noninteraction case, where sublattice B remained unpopulated owing to the chiral symmetry of the Hamiltonian, the introduction of interaction changes this dynamic. As the interaction strength increases, sublattice B becomes progressively more populated, which, in turn, reduces the population of

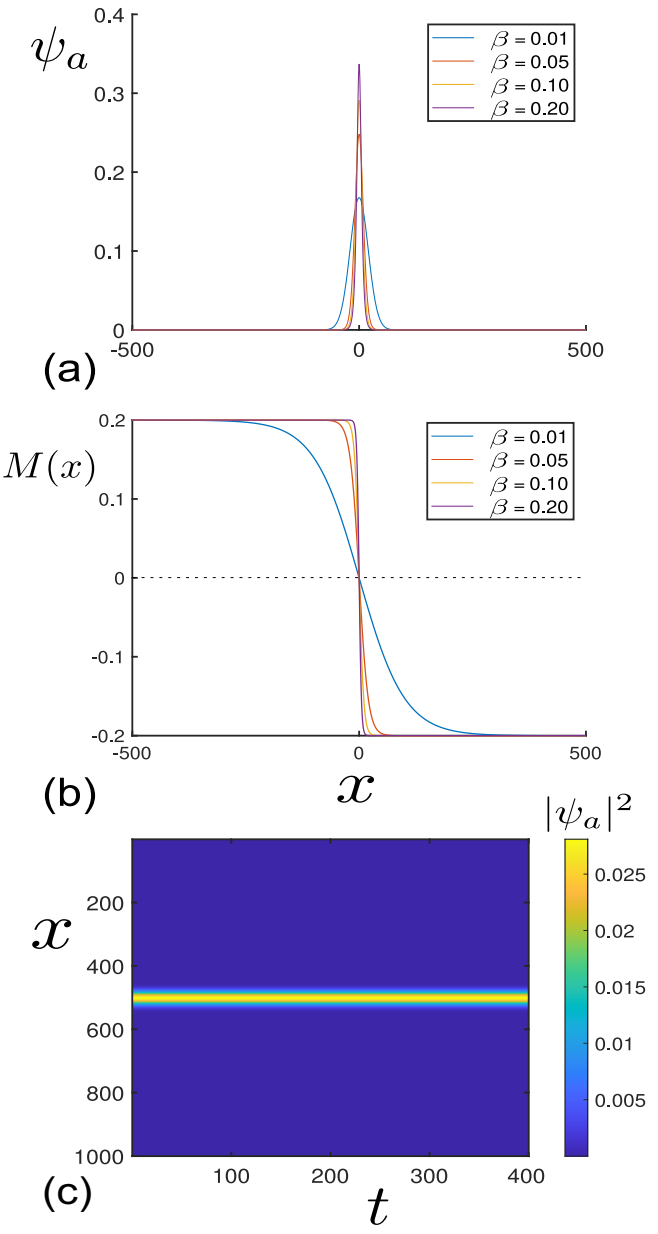

FIG. 2. (a) Displays the variation of the boundary states ψ_a corresponding to sublattice A as a function of the parameter β, which characterizes the steepness of the domain wall shown in (b). (c) Probability density of the numerically obtained boundary state wave function ψ_a corresponding to sublattice A, plotted as a function of real-time t. The wave function is for the case $\beta = 0.01$ and $\alpha' = 0$. The color scale indicates the magnitude of the probability density, which remains constant during the evolution.

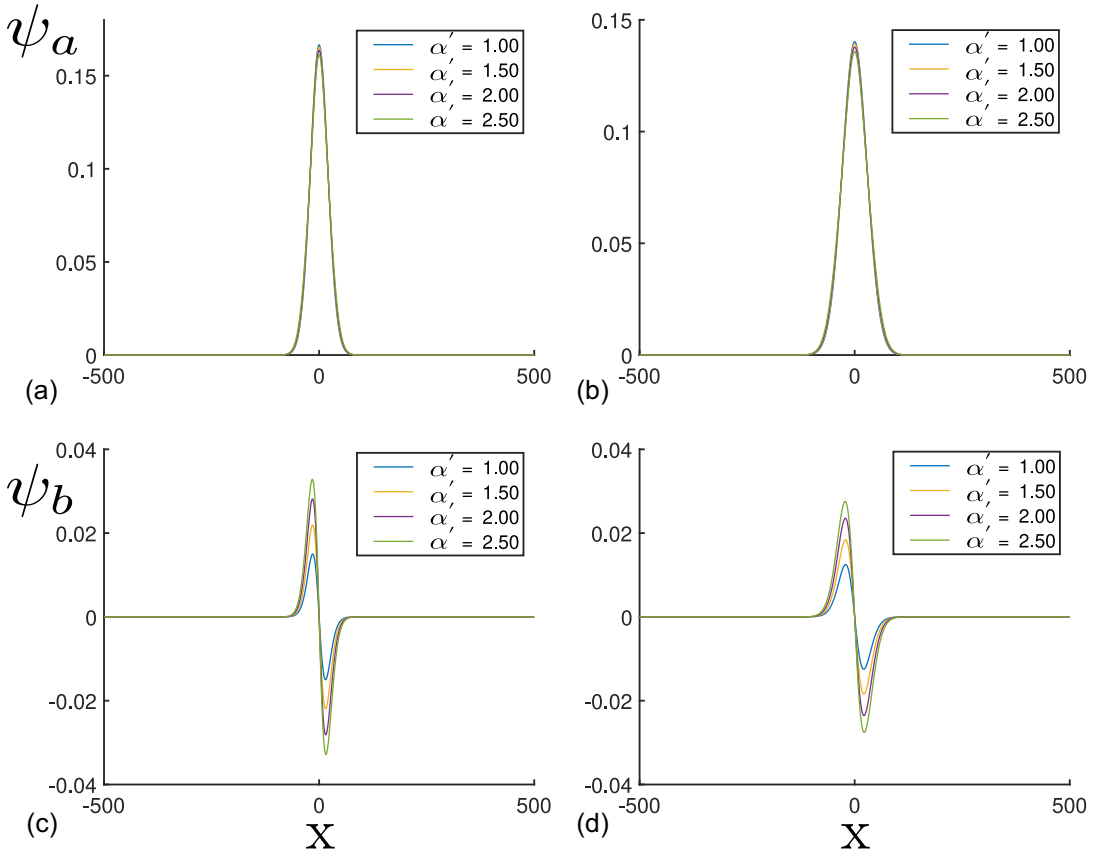

FIG. 3. The impact of interaction on boundary states for two levels of boundary stiffness is illustrated. The two columns depict different boundary sharpness values: $\beta = 0.01$ for the left column and $\beta = 0.005$ for the right column. The rows ((a), (b) and (c), (d)) show the boundary wavefunctions for sublattices A and B, respectively. With increasing interaction parameter α', the population in sublattice B increases.

sublattice A, see Fig. 3. The SSH nature of the parent Hamiltonian tends to confine the wavefunction to the A sublattice. However, increasing the interaction strength counters this tendency. Since a localized wavefunction results in higher potential energy, the system tends to delocalize by occupying sublattice B to lower the potential energy. This effect is similar to what is observed in the Gross-Pitaevskii equation, where, with the increase in the interaction, the central maxima of the ground-state wave function decreases and flattens in order to compensate for the increased potential energy from repulsive interactions [32]. In the typical Gross Pitaevskii equation, the external trap of harmonic potential is the factor that tries to localize the wavefunction, whereas, in this system, it is the topological barrier. A competition between the interaction and the topological barrier determines the structure of the wavefunction.

B. Analogous physical system

Here, we consider a physically intuitive and experimentally feasible system to visualize the results obtained in Subsec. A of this section. The system consists of an ultracold boson gas confined in a periodic potential well with alternating amplitudes, truncated at both ends by a step potential, as illustrated in Fig. 4. The behavior of ultracold bosons in a trap is governed by the Gross-Pitaevskii equation, a nonlinear partial differential equation that describes the macroscopic wave function of the condensate. In its dimensionless form,

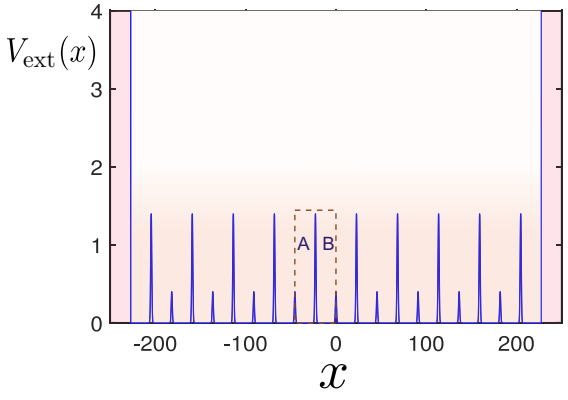

FIG. 4. Schematic diagram of the system. Inside the box, sharp Gaussian potentials with alternating amplitudes are applied, while the box itself is characterized by higher step-like potentials. This configuration forms two sublattices (A and B) with staggered tunneling amplitudes between the sites and open boundary conditions at the edges. The gradated cream color is a cartoon representation of the region containing ultracold bosonic gas, while the light pink stripes at the ends denote the open boundaries.

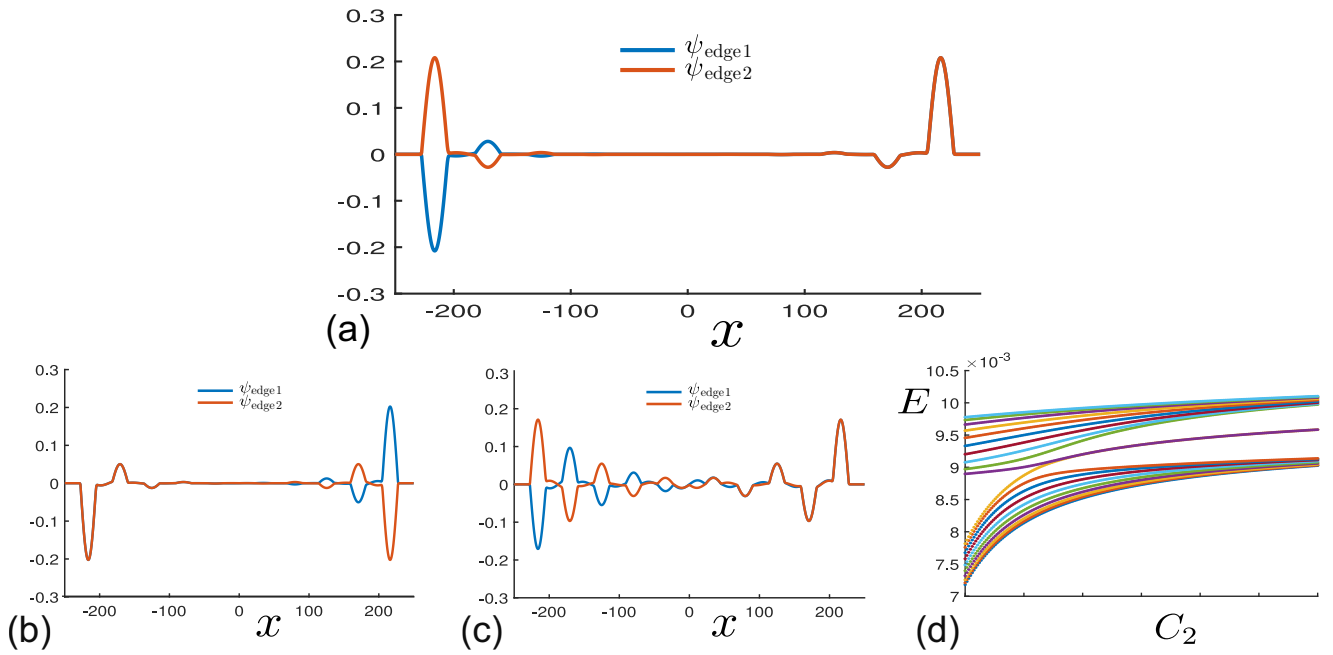

FIG. 5. lllustrates the system's analogy to the SSH model. (a) shows highly localized edge states reflecting the effect of chiral symmetry in the SSH system, with the left edge confined to the first sublattice and the right to the second. Panels (a)–(c) depict the evolution as C_2 (the amplitude of V_2) decreases, from greater than C_1 (fixed at 0.4) to approaching similar values: (a) $C_2 = 1.4$, (b) $C_2 = 1.0$, (c) $C_2 = 0.6$, with $d = 0.004$ for all cases. The energy diagram in (d) shows edge states within the mid-gap after band closure, calculated from the eigenvalue solution using finite differences.

the 1D Gross-Pitaevskii equation is given by

$$i\frac{\partial\psi}{\partial t} = \left(-\frac{\partial^2}{\partial x^2} + V_{\text{ext}}(x) + g|\psi|^2\right)\psi, \tag{16}$$

with ψ is the macroscopic wavefunction, V_{ext} is the externally applied potential, and g is the interaction strength [32,33]. The periodic structure with a series of equidistant alternating potentials is formed by sharp Gaussians with two corresponding amplitudes,

$$V_{1(2)}(x) = C_{1(2)}e^{-d(x-\mu)^2}, \tag{17}$$

whereas the ends are modeled by step potentials V_{step}, with a magnitude significantly larger than $C_{1(2)}$. The total form of potentials is given by

$$V_{\text{ext}} = \sum_{n=2}^{N_{\text{pot}}-1} [V_2[1 - \text{mod}(n, 2)] + V_1[\text{mod}(n, 2)]] + V_{\text{step}}[\delta_{1,n} + \delta_{N_{\text{pot}},n}], \tag{18}$$

where N_{pot} is the total number of potentials including those of the boundary, represented by indices $n = 1$ and $n = N_{\text{pot}}$. The system represents the physical picture corresponding to the model considered in the previous section for several reasons. The system is set up in an ultracold environment, leading to low-energy states. The alternating potentials [illustrated in Fig. 4 and defined in Eq. (18)] generate SSH-like staggered quantum tunneling amplitudes [Eq. (1)], leading to the formation of two sublattices (A and B). The high step potentials at the boundaries mimic the open boundaries of a finite SSH system.

The properties arising as a result of this configuration confirm that of SSH-like Hamiltonian, as is demonstrated in Fig. 5. It hosts edge states, i.e., highly localized states at the edges, with each side (right and left) residing on a particular sublattice, i.e., the left edge resides on sublattice A, and the right edge resides on sublattice B [particularly refer to Fig. 5(a)]. As the staggered quantum tunneling amplitude becomes more uniform, the edge states progressively delocalize, as shown in Figs. 5(a)–5(c). These edge states have energies within the band gap, and as the tunneling becomes equal, the edge states merge with the bulk, causing the energy band to close at the transition point, as illustrated in Fig. 5(d). The topology associated with this kind of alternating potential has been experimentally confirmed [34] and theoretically studied [35].

Now, we proceed to investigate the boundary states with the interactions present. Since the boundary states are not the lowest eigenstates in the system, we use the ITPUSH algorithm developed in Sec. III to study them. The ψ_0 and E_0 required for this algorithm are obtained by solving the finite-difference eigenvalue problem when no interaction is present. Then, we gradually increase the interaction strength and study the boundary wavefunction for each case. Figure 6 shows the wavefunctions corresponding to different interaction strengths for the configuration corresponding to the wavefunction in Fig. 5(a). These results closely align with those obtained through the continuum mechanics approach discussed in the previous subsection. It may be noted from Fig. 6 that the interactions have the effect of flattening the edge state, i.e., the amplitude of the wavefunction at the boundary reduces, and it extends further into the bulk. Another notable effect

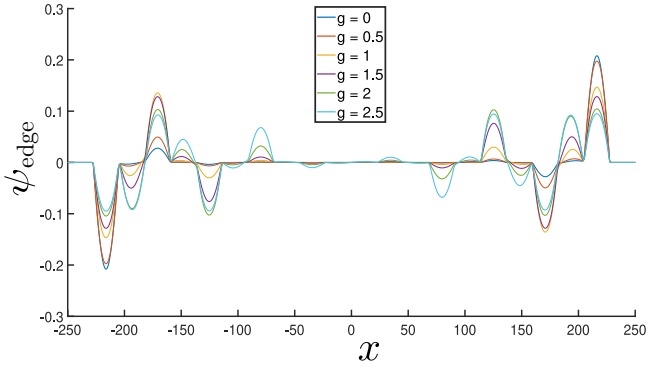

FIG. 6. Effect of interactions on boundary wavefunctions. Interactions reduce the wavefunction amplitude at the boundary and enable occupation of sublattices previously restricted by the SSH-like nature of the system, with occupation increasing as interaction strength grows (denoted by g).

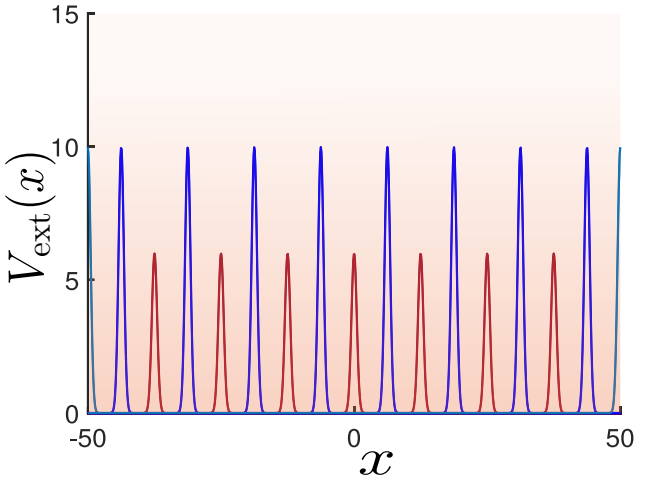

FIG. 7. Schematic illustration of the system. The deep wells with alternating amplitudes (V_1 and V_2) result in alternating hopping amplitudes, with the boundary potential set to V_1.

is populating the sublattice that was previously unoccupied in the noninteracting SSH type system, i.e., the B sublattice for the left edge and the A sublattice for the right edge. The occupation of these previously empty sublattices increases progressively with an increase in interaction. These effects align with the findings in Sec. IV A, where the occupation of sublattice B increases with interaction strength, leading to a reduction in occupation on sublattice A. However, this reduction is not very apparent in Fig. 3 owing to the difference in magnitude between the two sublattices. The momentum-space wavefunctions corresponding to the boundary states computed in this section, as shown in Figs. 5 and 6, are confined to a k-space region significantly smaller than π. This allows a valid comparison between the overall envelope of these boundary states and those obtained in the previous section using the envelope-function approximation. It is worth noting that with this form of potential, which creates staggered tunneling amplitudes, depending on how the boundary is constructed, there may exist other boundary states that do not exhibit the topological nature of the SSH-type Hamiltonian. These states, along with the effects of interactions on them, are examined in Appendix.

V. SUMMARY AND CONCLUSIONS

Building on the imaginary-time propagator method, we have developed an algorithm to target specific eigenstates within a spectrum. This algorithm requires an initial guess for both the trial wavefunction and energy, then evolves the wavefunction in imaginary time using a squared Hamiltonian to converge to the desired state. We applied this approach to investigate the effects of interactions on boundary states of bosons in an SSH lattice within ultracold environments.

First, using the continuum approximation, we derived an effective Hamiltonian via the functional minimization of a mean-field energy functional. The algorithm was then used to identify boundary states in the energy spectrum, which included both positive and negative values. Initially, the method was applied to noninteracting bosons, confirming well-known states across varying levels of boundary sharpness. Next, boundary states were examined under varying interaction strengths, revealing that interactions enhance population on the B sublattice while reducing it on the A sublattice.

We then explored a physical model with analogous characteristics representing the theoretical continuum model: ultracold bosons trapped in a box containing periodic potential structure with alternating amplitudes. First, the system's properties were examined in the noninteracting regime, drawing an analogy to the SSH model regarding edge states and energy structure. Using the developed algorithm, we then investigated the effect of incorporating interactions into the system on the boundary states. A notable impact of incorporating interactions into the system is that it allows occupation of sublattices previously constrained by the SSH nature of the potentials, with this occupation increasing as the interaction strength grows. This behavior aligns with the continuum theory of the problem. Additionally, the interaction causes a reduction in the edge state's amplitude at the boundary, while simultaneously promoting its spread into the bulk.

ACKNOWLEDGMENT

A.G. acknowledges the University of Melbourne and the Indian Institute of Technology Kharagpur for institutional support during this research. A.G. was supported by institute scholarship from IIT Kharagpur, the Government of India, and the Melbourne Research Scholarship.

APPENDIX: ADDITIONAL TYPES OF BOUNDARY STATES AND THE IMPACT OF INTERACTIONS

In this Appendix, we discuss the impact of interactions on boundary states, which differ from those discussed in the main text, which reflected the topological character of the edge states of the SSH type Hamiltonian, i.e., a mid-band positioned with selective sublattice occupation. The potentials considered here have roughly the same form, consisting of alternating potentials [as in Eq. (17)], except the boundary potentials have the same height as that of one of the inner peri-

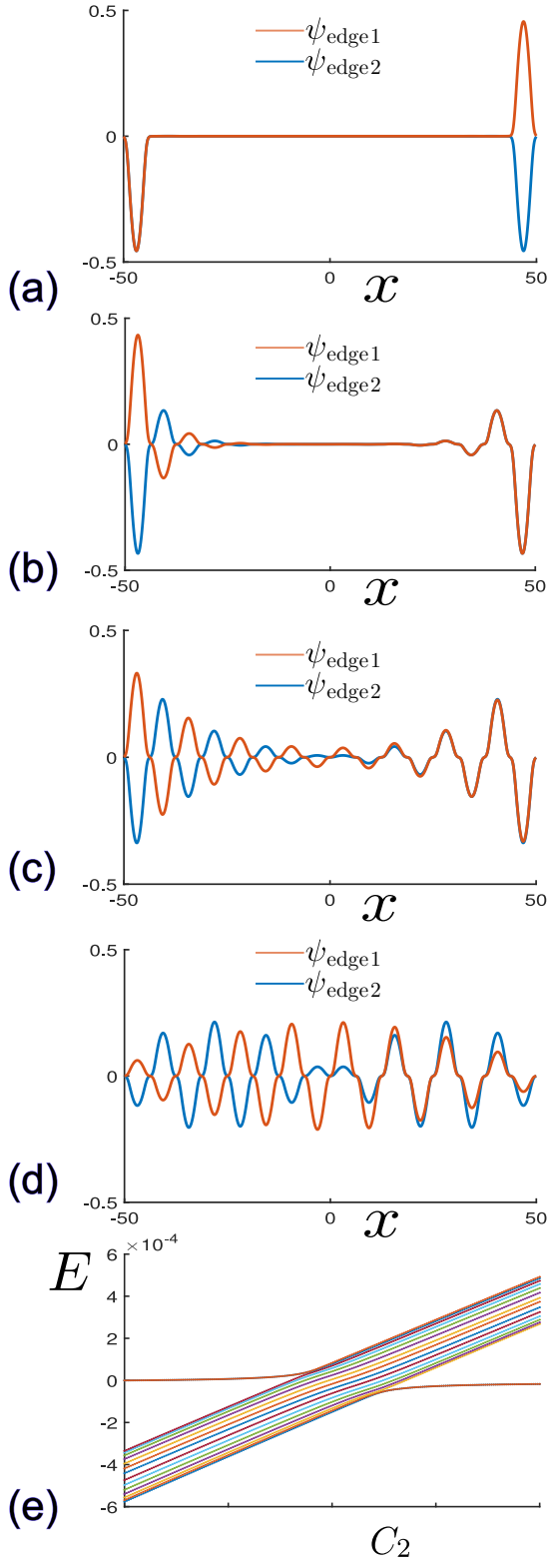

FIG. 8. Boundary states' behavior as staggered nature of the potentials are reduced. Panels (a)–(d) illustrate the progression with increasing C_2 (from 0 to 9.97, with C_1 fixed at 9.97, and d fixed at 0.005), resulting in uniform hopping. Panel (e) displays the energy diagram from the finite difference method, indicating that boundary states remain isolated for $C_2 < C_1$ and a new boundary state appears when $C_2 = C_1$. The lack of sublattice specificity and energy locations differs from the SSH-type Hamiltonian's topological features.

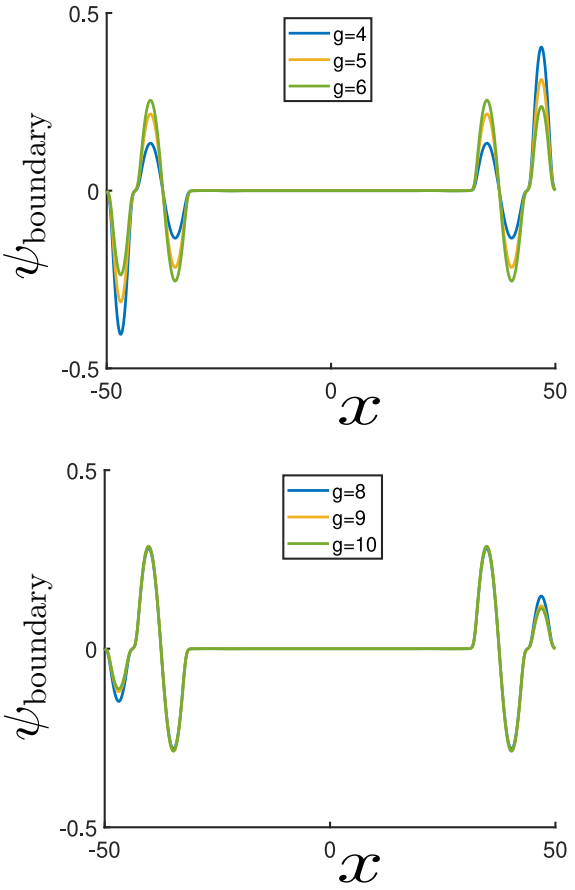

FIG. 9. The impact of interactions on the boundary wavefunctions. (a) shows the boundary wavefunctions for interactions $g = \{4, 5, 6\}$, and (b) for $g = \{8, 9, 10\}$. A gradual flattening of the boundary wavefunctions is observed with increasing interactions.

odic potentials (V_1), as illustrated in Fig. 7. The mathematical expression is

$$V_{\text{ext}} = \sum_{n=2}^{N_g-1} [V_1[1 - \text{mod(n, 2)}] + \text{V}_2[\text{mod(n, 2)}]] + V_1[\delta_{1,n} + \delta_{N_g,n}], \tag{A1}$$

where N_g represents the total number of Gaussians, including the boundary terms. For the above choice of potentials, the energies of these states match those of the bulk states when $V_1 = V_2$, and as a result they gradually delocalize in the bulk as V_1, approaches V_2. Figure 8 illustrates this process, (a)–(d) show the gradual delocalization of these states into the bulk, while (e) represents the corresponding energies, where the distinct higher energies correspond to these energy states (rescaled to maintain the boundary state energy at zero). However, these states may have energies significantly higher or lower than those of the bulk states depending on the form of boundaries, preventing their merging with the bulk in such cases.

Turning to the effect of interactions on these boundary states, we again utilize the ITPUSH algorithm introduced in Sec. III of the main text to study them, since these boundary states correspond to the highest eigenstates within the con-

sidered energy band. As before, the initial wavefunction ψ_0 and energy E_0 required for this algorithm are obtained by solving the finite-difference eigenvalue problem in the non-interacting case. The interaction is then gradually introduced within the Gross-Pitaevskii framework [Eq. (16)], and the boundary wavefunctions are analyzed. Figure 9 presents the wavefunctions corresponding to various interaction strengths. It can be observed that interactions cause the wavefunctions to spread, distributing in a manner that minimizes the increased potential energy.

[1] M. Z. Hasan and C. L. Kane, *Colloquium:* Topological insulators, Rev. Mod. Phys. **82**, 3045 (2010).

[2] S. Rachel, Interacting topological insulators: A review, Rep. Prog. Phys. **81**, 116501 (2018).

[3] N. Goldman, J. C. Budich, and P. Zoller, Topological quantum matter with ultracold gases in optical lattices, Nat. Phys. **12**, 639 (2016).

[4] O. Dmytruk and M. Schirò, Controlling topological phases of matter with quantum light, Commun. Phys. **5**, 271 (2022).

[5] A. Ghosh, A. M. Martin, and S. Majumder, Quench dynamics of edge states in a finite extended Su-Schrieffer-Heeger system, Phys. Rev. E **108**, 034102 (2023).

[6] J. K. Asbóth, L. Oroszlány, and A. Pályi, *A Short Course on Topological Insulators*, Lecture Notes in Physics, Vol. 919 (Springer, New York, 2016), pp. 1–166.

[7] S.-Q. Shen, *Topological Insulators* (Springer, New York, 2012), Vol. 174.

[8] B. A. Bernevig, *Topological Insulators and Topological Superconductors* (Princeton University Press, Princeton, 2013).

[9] C. L. Kane and E. J. Mele, Quantum spin Hall effect in graphene, Phys. Rev. Lett. **95**, 226801 (2005).

[10] C. L. Kane and E. J. Mele, Z_2 topological order and the quantum spin Hall effect, Phys. Rev. Lett. **95**, 146802 (2005).

[11] W. A. Benalcazar, B. A. Bernevig, and T. L. Hughes, Quantized electric multipole insulators, Science **357**, 61 (2017).

[12] F. Schindler, A. M. Cook, M. G. Vergniory, Z. Wang, S. S. P. Parkin, B. A. Bernevig, and T. Neupert, Higher-order topological insulators, Sci. Adv. **4**, eaat0346 (2018).

[13] G. Jotzu, M. Messer, R. Desbuquois, M. Lebrat, T. Uehlinger, D. Greif, and T. Esslinger, Experimental realization of the topological Haldane model with ultracold fermions, Nature (London) **515**, 237 (2014).

[14] J. Léonard, S. Kim, J. Kwan, P. Segura, F. Grusdt, C. Repellin, N. Goldman, and M. Greiner, Realization of a fractional quantum Hall state with ultracold atoms, Nature (London) **619**, 495 (2023).

[15] D. Hsieh, Y. Xia, D. Qian, L. Wray, F. Meier, J. H. Dil, J. Osterwalder, L. Patthey, A. V. Fedorov, H. Lin, A. Bansil, D. Grauer, Y. S. Hor, R. J. Cava, and M. Z. Hasan, Observation of time-reversal-protected single-Dirac-cone topological-insulator states in Bi_2Te_3 and Sb_2Te_3, Phys. Rev. Lett. **103**, 146401 (2009).

[16] M. König, S. Wiedmann, C. Brune, A. Roth, H. Buhmann, L. W. Molenkamp, X.-L. Qi, and S.-C. Zhang, Quantum spin Hall insulator state in HgTe quantum wells, Science **318**, 766 (2007).

[17] S. De Léséleuc, V. Lienhard, P. Scholl, D. Barredo, S. Weber, N. Lang, H. P. Büchler, T. Lahaye, and A. Browaeys, Observation of a symmetry-protected topological phase of interacting bosons with Rydberg atoms, Science **365**, 775 (2019).

[18] J.-X. Yin, S. H. Pan, and M. Z. Hasan, Probing topological quantum matter with scanning tunnelling microscopy, Nat. Rev. Phys. **3**, 249 (2021).

[19] L. Peng, Y. Yuan, G. Li, X. Yang, J.-J. Xian, C.-J. Yi, Y.-G. Shi, and Y.-S. Fu, Observation of topological states residing at step edges of WTe_2, Nat. Commun. **8**, 659 (2017).

[20] P. Zhang, K. Yaji, T. Hashimoto, Y. Ota, T. Kondo, K. Okazaki, Z. Wang, J. Wen, G. D. Gu, H. Ding *et al.*, Observation of topological superconductivity on the surface of an iron-based superconductor, Science **360**, 182 (2018).

[21] E. Nicolau, A. M. Marques, J. Mompart, R. G. Dias, and V. Ahufinger, Bosonic orbital Su-Schrieffer-Heeger model in a lattice of rings, Phys. Rev. A **108**, 023317 (2023).

[22] E. J. Meier, F. Alex An, and B. Gadway, Observation of the topological soliton state in the Su–Schrieffer–Heeger model, Nat. Commun. **7**, 13986 (2016).

[23] L. Lu, J. D. Joannopoulos, and M. Soljačić, Topological photonics, Nat. Photon. **8**, 821 (2014).

[24] J. Paulose, B. Gin-ge Chen, and V. Vitelli, Topological modes bound to dislocations in mechanical metamaterials, Nat. Phys. **11**, 153 (2015).

[25] C. H. Lee, S. Imhof, C. Berger, F. Bayer, J. Brehm, L. W. Molenkamp, T. Kiessling, and R. Thomale, Topolectrical circuits, Commun. Phys. **1**, 39 (2018).

[26] W.-P. Su, J. R. Schrieffer, and A. J. Heeger, Solitons in polyacetylene, Phys. Rev. Lett. **42**, 1698 (1979).

[27] D. Mikhail, B. Voisin, D. D. St Medar, G. Buchs, S. Rogge, and S. Rachel, Quasiparticle excitations in a one-dimensional interacting topological insulator: Application for dopant-based quantum simulation, Phys. Rev. B **106**, 195408 (2022).

[28] F. Grusdt, M. Höning, and M. Fleischhauer, Topological edge states in the one-dimensional superlattice Bose-Hubbard model, Phys. Rev. Lett. **110**, 260405 (2013).

[29] T. Tuloup, R. W. Bomantara, C. H. Lee, and J. Gong, Nonlinearity induced topological physics in momentum space and real space, Phys. Rev. B **102**, 115411 (2020).

[30] M. Horvath, S. Dhar, A. Das, M. D. Frye, Y. Guo, J. M. Hutson, M. Landini, and H.-C. Nägerl, Bose-Einstein condensation of non-ground-state caesium atoms, Nat. Commun. **15**, 3739 (2024).

[31] H. Takayama, Y. R. Lin-Liu, and K. Maki, Continuum model for solitons in polyacetylene, Phys. Rev. B **21**, 2388 (1980).

[32] F. Dalfovo and S. Stringari, Bosons in anisotropic traps: Ground state and vortices, Phys. Rev. A **53**, 2477 (1996).

[33] C. J. Pethick and H. Smith, *Bose–Einstein Condensation in Dilute Gases* (Cambridge University Press, Cambridge, 2008).

[34] M. Atala, M. Aidelsburger, J. T. Barreiro, D. Abanin, T. Kitagawa, E. Demler, and I. Bloch, Direct measurement of the Zak phase in topological Bloch bands, Nat. Phys. **9**, 795 (2013).

[35] T. B. Smith, C. Kocabas, and A. Principi, Topological plasmonic waveguides in triharmonic metal gratings, J. Phys.: Condens. Matter **33**, 265003 (2021).